Multifaceted activity of polyciclic MDR revertant agents in drug-resistant leukemic cells: Role of the spacer

# MULTIFACETED ACTIVITY OF POLYCICLIC MDR REVERTANT AGENTS IN DRUG-RESISTANT LEUKEMIC CELLS: ROLE OF THE SPACER

Jessica Caciolla,[a] Giovanna Picone,[b] Giovanna Farruggia,[b, c] Dario Valenti,[a, 1] Angela Rampa,[a] Emil Malucelli,[b] Federica Belluti,[a] Alfonso Trezza,[e] Ottavia Spiga,[e] Stefano Iotti,[b, c] Silvia Gobbi,[a] Concettina Cappadone,[b]* Alessandra Bisi[a]**

[a]*Department of Pharmacy and Biotechnology, Alma Mater Studiorum-University of Bologna, Via Belmeloro 6, 40126 Bologna, Italy;* [b]*Department of Pharmacy and Biotechnology, Alma Mater Studiorum-University of Bologna, Via S. Donato 19/2, 40127 Bologna, Italy;* [c]*National Institute of Biostructures and Biosystems, Via delle Medaglie D'oro, 305, 00136 Roma, Italy,* [e]*Department of Biotechnology, Chemistry and Pharmacy, University of Siena, Siena, 53100, Italy*

Corresponding Authors

* E-mail: concettina.cappadone@unibo.it.** E-mail: alessandra.bisi@unibo.it

[1] Present address: Medicinal Chemistry, Taros Chemicals GmbH & Co. KG, Emil-Figge-Straße 76a, Dortmund, Germany

**Abbreviations**

MDR, multidrug resistance; ABC, ATP-binding cassette; P-gp, P-glycoprotein; MRP-1, multidrug resistance-associated protein 1; BCRP, breast cancer resistance protein; TMD, transmembrane domain; NBD, nucleotide-binding domain; GS-X pump, glutathione S-conjugate export pump; DBP,

drug-binding pocket; CS, collateral sensitivity; DMSO, dimethylsulfoxide; CuAAC, copper (I) catalysed azide-alkyne cycloaddiction; *t*-BuOK, potassium ter-butoxide; R123, rhodamine123.

**Abstract**

A small library of derivatives carrying a polycyclic scaffold recently identified by us as a new privileged structure in medicinal chemistry was designed and synthesized, aiming at obtaining potent MDR reverting agents also endowed with antitumor properties. In particular, as a follow-up of our previous studies, attention was focused on the role of the spacer connecting the polycyclic core with a properly selected nitrogen-containing group. A relevant increase in reverting potency was observed, going from the previously employed but-2-ynyl- to a pent-3-ynylamino moiety, as in compounds **3d** and **3e**, while the introduction of a triazole ring proved to differently impact on the activity of the compounds. The docking results supported the data obtained by biological tests, showing, for the most active compounds, the ability to establish specific bonds with P-glycoprotein. Moreover, a multifaceted anticancer profile and dual in vitro activity was observed for all compounds, showing both revertant and antitumor effects on leukemic cells. In this respect, **3c** emerged as a "triple-target" agent, endowed with a relevant reverting potency, a considerable antiproliferative activity and a collateral sensitivity profile.

**Keywords**

P-glycoprotein, MDR modulators, HL60 cells, Collateral Sensitivity, Anticancer.

## 1. Introduction

Cancer is presently recognized as the most malignant disease and represents one of the major causes of death in most countries [1]. Mainly due to the aging of population, the mortality rates related to this pathology are continuously increasing worldwide. Significant progresses in cancer therapy have been made in the last decades, although the risk of tumours acquiring multidrug resistance (MDR) to chemotherapeutic drugs remains a huge drawback for an effective treatment of several types of cancers. Intrinsic or acquired MDR can be regarded as a sort of self-defence process that tumour cells develop against chemotherapeutic drugs, characterized by the onset of cross-resistance toward multiple chemically and mechanistically unrelated drugs [2]. Several mechanisms are involved in the emergence of MDR, among which altered membrane transport, namely increasing drug efflux or decreasing drug uptake, remains the most investigated. Indeed, the overexpression of energy-dependent ATP-binding cassette (ABC) transporter proteins, able to pump anticancer drugs outside the cells, represents a distinctive and highly conserved feature of resistant cancer cells. The human ABC superfamily counts at least 48 efflux pumps that play a pivotal role in detoxifying cells from both metabolites generated by conventional cellular processes and exogenous toxic agents, including chemotherapeutic drugs, thus giving rise to the resistance mechanism. Among these transporters, P-glycoprotein (P-gp, MDR1, or ABCB1), multidrug resistance-associated protein 1 (MRP1 or ABCC1) and breast cancer resistance protein (BCRP, ABCG2) are mainly connected to the onset of MDR [3]. P-gp, a 170 kDa protein, is undoubtedly the most studied ABC transporter, structurally classified as a pseudosymmetrical heterodimer, in which each monomer is formed by six transmembrane domains (TMD), involved in substrates recognition and transport, and one nucleotide-binding domain (NBD), responsible for ATP binding and hydrolysis [4]. MRP1 can be defined as an ATP-dependent glutathione S-conjugate export pump (GS-X pump), thus acting with

a completely different mechanism from that of P-gp mediated resistance [5]. Nevertheless, most of the anticancer drugs extruded by P-gp are also substrates for MRP1. BCRP, the most recently identified ABC transporter, has been recognized in a number of hematological and solid tumours, mainly together with P-gp. A tentative strategy to circumvent MDR can be the co-administration of the antitumor drug with a reversal agent, able to engage the transporter, thus restoring the sensitivity of resistant neoplastic cells [6]. Unfortunately, this approach did not attain appreciable efficacy in clinical trials, mainly due to dose-limiting toxicity and unpredictable pharmacokinetic interactions. However, the search for new efflux pumps modulators still holds a significant interest, because of the need for a better understanding of the mechanisms of action of these proteins. Notably, a pivotal role for P-gp and other transporters was also recognized in brain disorders, such as Alzheimer's disease and Parkinson disease, where a decrease in their expression and function at blood brain barrier level has been reported [7].

A large number of synthetic and natural compounds able to counteract the activity of these transporters has been reported in the last years, from the first-generation calcium channels modulators verapamil, flunarizine and lomerizine to the third-generation tariquidar [8] and zosuquidar [9] (Figure 1), showing a remarkable structural dissimilarity that can be related to the structural features of P-gp, the most studied efflux pump. Indeed, the crystal structure of murine P-gp, (with 87 % sequence identity to human P-gp) identified a large hydrophobic chamber near the periplasmatic lipid bilayer interface as a possible drug-binding pocket (DBP), where different compounds can adapt in many different ways. Anyway, some typical common features for appropriate binding to this protein have been recognized, such as the presence of a protonable nitrogen and aromatic rings, together with groups able to establish H-bond interactions and an overall high lipophilicity of the whole structure [4,10]. An alternative strategy to combat MDR

could be the identification of small molecules able to selectively kill resistant cells, rather than the sensitive ones, a phenomenon identified as collateral sensitivity (CS). Compounds endowed with this ability could then resensitize resistant tumors towards chemotherapeutic treatment and/or reduce MDR occurrence through co-administration with standard antitumor drugs. [11]

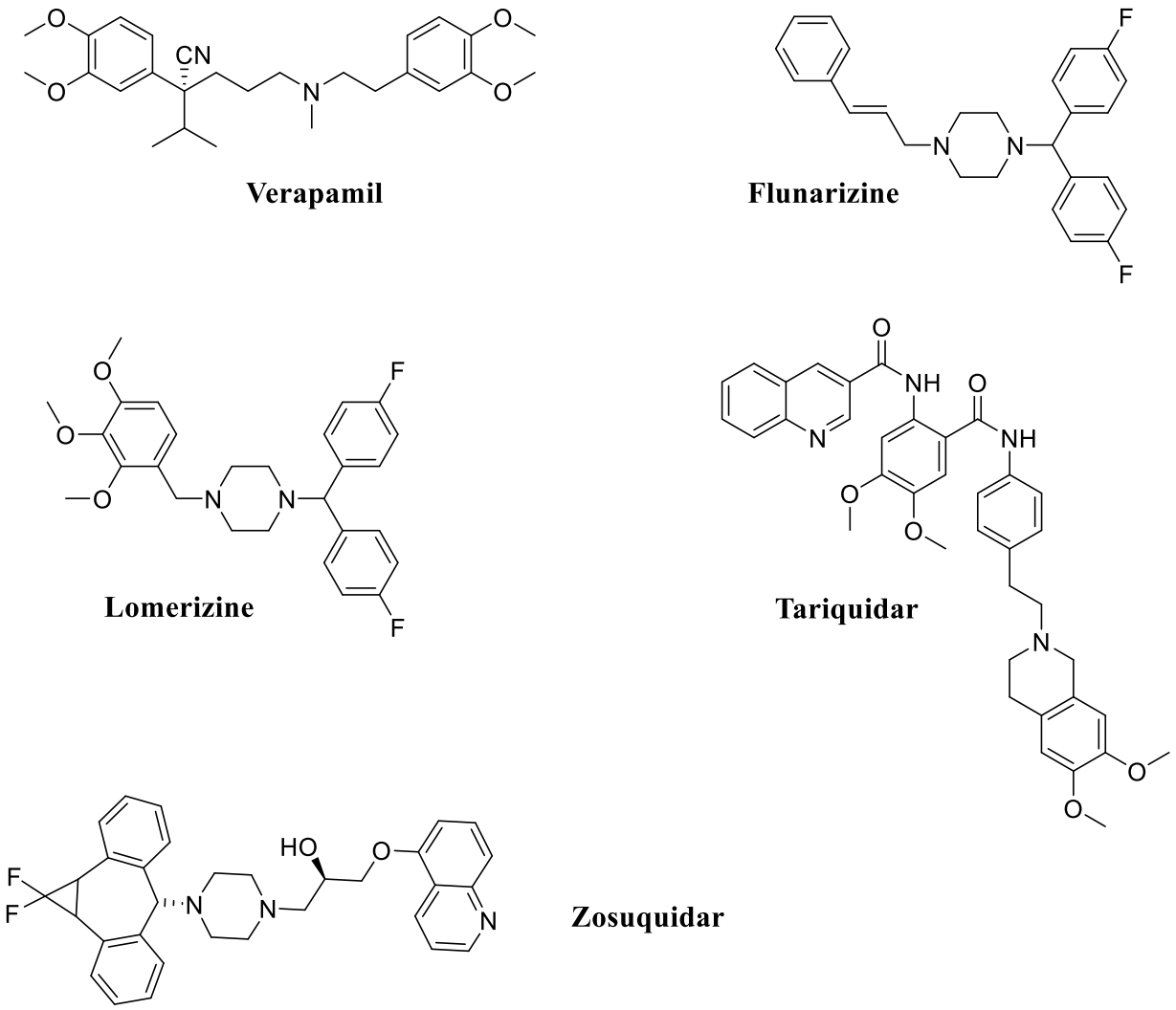


**Figure 1.** Representative MDR reversal agents.

In previous papers [12,13] we identified a series of new potent multifaceted anticancer and MDR reverting compounds carrying an easily affordable and previously unexplored polycyclic scaffold,

selected on the basis of its peculiar structure: bearing aromatic residues and carbonyl groups, it could provide both good π orbitals overlapping and H-bond accepting properties. Notably, we have recently recognized this core as a new "privileged structure", a simple structural subunit able to bind different targets and/or modulate its biological profile, when properly decorated. [14-16] In particular, among this series, compounds **1** and **2** (Figure 2), bearing a rigid but-2-ynyl side chain and a 3,4-dimethoxyphenetyl(methyl)amine moiety, related to the structure of verapamil, or a bis (4-fluorophenyl) methyl piperazinyl moiety, related to flunarizine and lomerizine, respectively, proved to be the most promising derivatives. Notably, flunarizine and lomerizine share with zosuquidar a piperazine fragment, recognized as a privileged structure in medicinal chemistry [17].

The two derivatives were selected as lead compounds based on their different biological profiles, being **1** a very potent and non-cytotoxic reverting agent, and showing **2** a multifaceted effect, i.e. a direct cytotoxicity coupled to significant MDR reverting activity, ten-fold higher than verapamil. Moreover, we also reported a series of phenothiazine derivatives bearing the same but-2-ynyl side chain, endowed with both reversal activity and a peculiar pharmacological profile [18].

In this study, the polycyclic scaffold and the terminal moieties (A and B, Figure 2) of **1** and **2** were maintained, and particular attention was given to assess the role of the spacer connecting these units, to evaluate the structural features involved in the optimal interaction with P-gp and MRP-1 and in the antitumor effects of these derivatives. In detail, i) the but-2-ynyl amino linker was modified by a click chemistry approach, thus introducing a 1,2,3-triazole ring suitable for maintaining a substantial structural rigidity, while integrating the nitrogen atom into an aromatic cycle (**3a-c**, Figure 2). This modification, by including the *N*-methyl amino function in the less basic triazole ring, enabled the evaluation of the impact of the amino group in side chain B, whose ability to protonate is considered to play a pivotal role in P-gp inhibition. Interestingly, this

nitrogen-containing heterocycle, extensively exploited as bioisostere of amide, ester and *trans*-olefinic bond [19], has also been proposed as a possible bioisostere of the ethynyl group [20] and could establish additional noncovalent interactions with the biological targets, namely hydrophobic interactions and hydrogen bonds, that have been recognized crucial for P-gp binding. The conjugation of this structure with an anticancer pharmacophore could then substantially contribute to the biological activity of the new compounds, increasing efficacy against resistant tumors and potentially providing new anticancer candidates. Indeed, this strategy has recently been widely explored by us and other groups [21, 22]. The role of the verapamil-like methoxy groups in the terminal aromatic ring was also evaluated by removing them in **3a**. ii) the elongation of the linker to five carbon atoms, from but-2-ynyl to pent-3-ynyl was also performed, leading to a slightly more flexible framework (compounds **3d, 3e**, Figure 2), in order to establish the optimal distance between the polycyclic core and the amine. Notably, this modification could also allow for a different positioning of the molecule with respect to the biological target. iii) the copper-catalysed click chemistry approach was differently exploited to modify the spacer (compounds **3f** and **3g**, Figure 2), keeping two methylene units between the core and the rigid moiety, as in compounds **3d** and **3e**, and also retaining the basic protonable function, unlike **3a-c**.

The new compounds were tested to evaluate their MDR-reverting activity and antiproliferative profile on acute myeloid leukemic HL60 cells and their MDR subline HL60R (obtained by continuous exposure to doxorubicin), expressing both P-gp and MRP-1. Moreover, a docking study was also performed in order to get insights into the possible binding mode of the new compounds to P-gp and to determine the structural features required for a significant inhibitory activity.

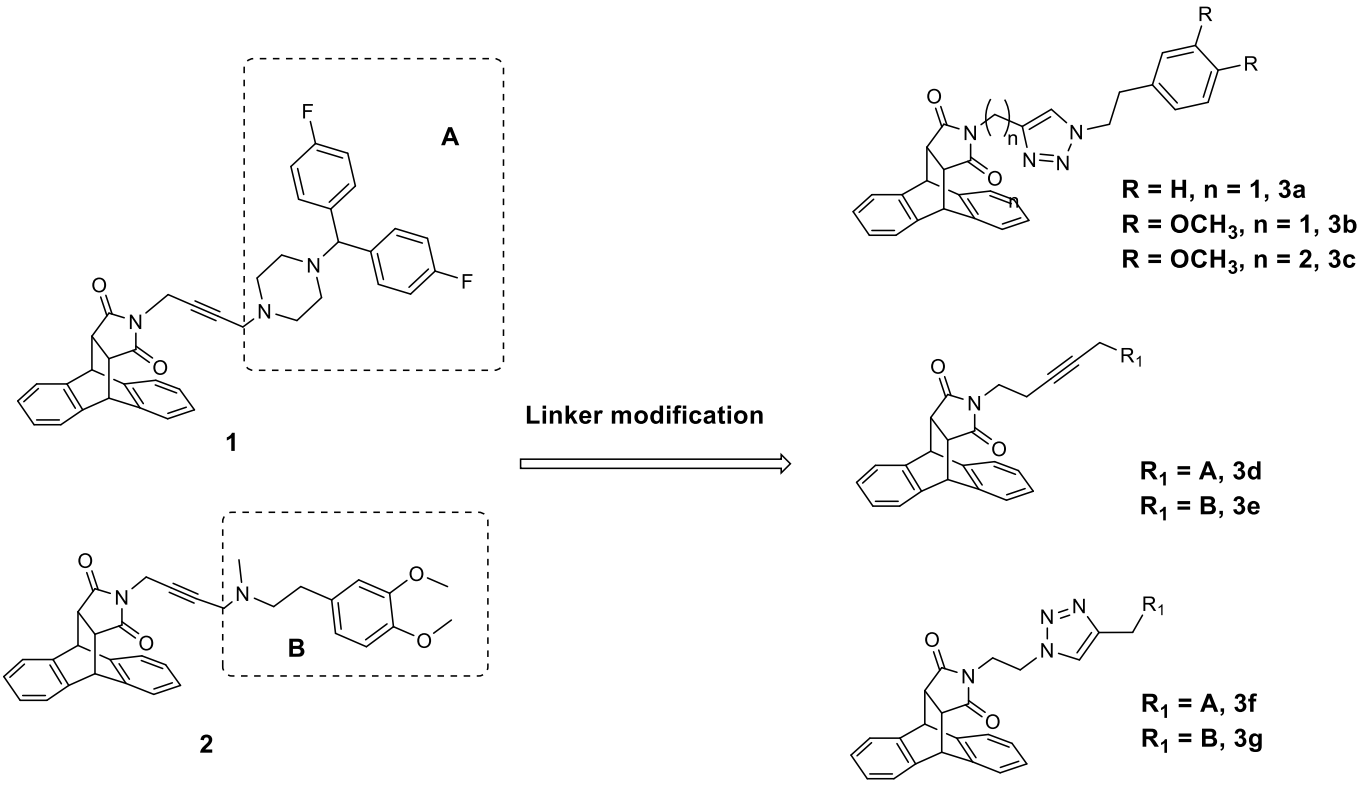


**Figure 2**. Design strategy for the new derivatives **3a-g**.

## 2. Results and discussion

### *2.1 Chemistry*

The designed compounds were prepared starting from the key intermediate 10,11-dihydro-9H-9,10-[3,4]epipyrroloanthracene-12,14(13H,15H)-dione (**4**), obtained by standard procedures [23] and then alkylated with the selected alkyl bromide, as depicted in Scheme 1, by means of potassium *tert*-butoxide in DMSO , to give **5** [23], **6**, and **7**. To obtain compounds **3a** and **3b**, intermediate **5** was submitted to copper (I) catalysed azide-alkyne cycloaddiction (CuAAC, "click" reaction) with (2-azidoethyl) benzene or 4-(2-azidoethyl)-1,2-dimethoxybenzene [24], in the presence of $CuSO_4$ and sodium ascorbate in DMSO. Compound **3c** was obtained with the same procedure starting from **6** and 4-(2-azidoethyl)-1,2-dimethoxybenzene. Derivatives **3d** and **3e** were attained starting from **6**, submitted to a Mannich reaction with the selected amine, in EtOH/$H_2O$ and in the presence of

$CuSO_4$ and formaldehyde. Finally, to obtain **3f** and **3g**, intermediate **7** was converted in the corresponding azide **8** by treatment with sodium azide in DMSO and then submitted to a CuAAC reaction with N-(3,4-dimethoxyphenethyl)-N-methylprop-2-yn-1-amine or 1-(bis(4-fluorophenyl)methyl)-4-(prop-2-yn-1-yl)piperazine.

**Scheme 1**. Synthesis of compounds **3a-g**.[a]

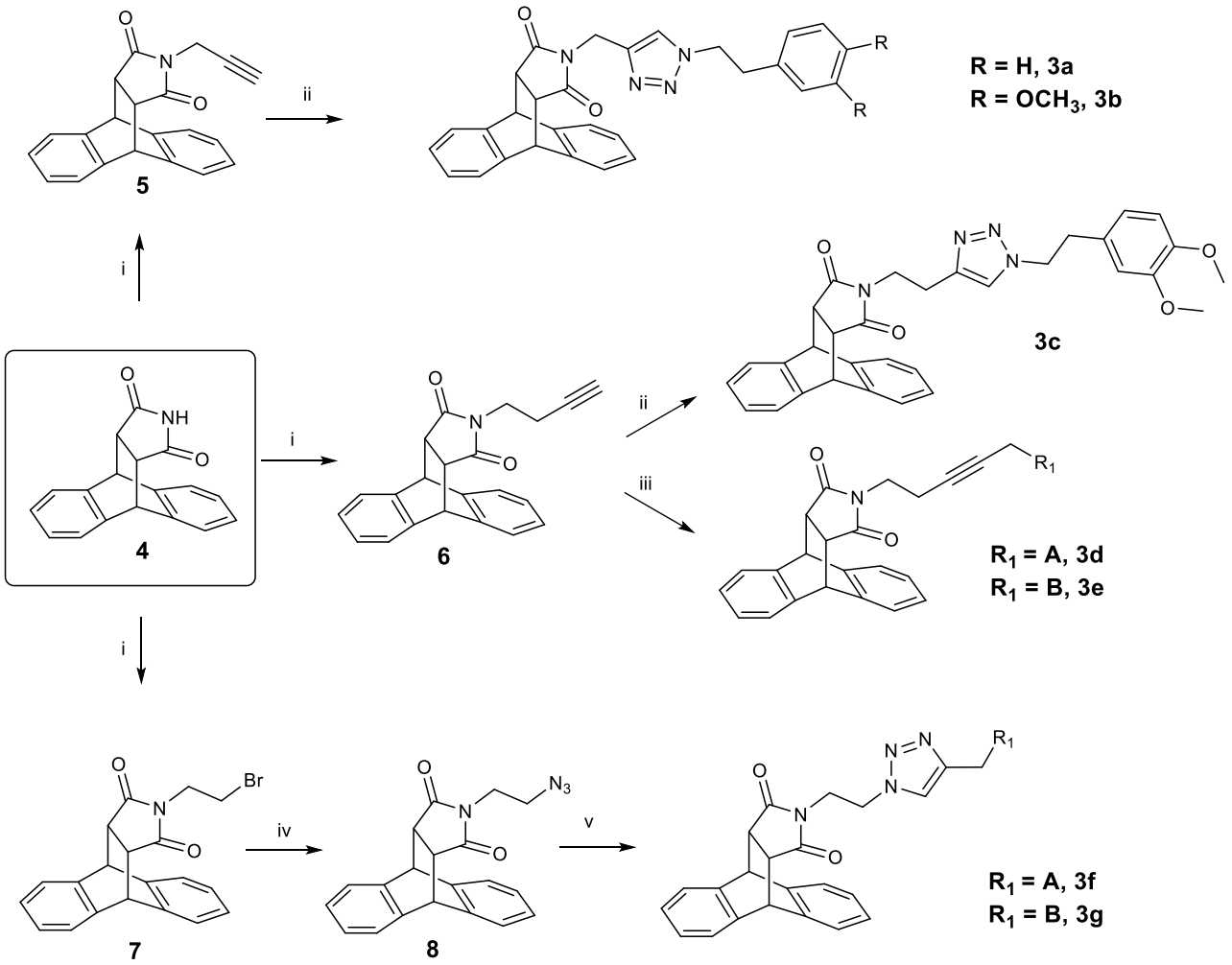


[a]**Reagents and conditions**: i) selected alkyl bromide, *t*-BuOK, DMSO, r.t., 2.5 h; ii) (2-azidoethyl)benzene (for **3a**) / 4-(2-azidoethyl)-1,2-dimethoxybenzene (for **3b** and **3c**), $CuSO_4$, Na

ascorbate, DMSO, 80-90 °C, 24 h; iii) 1-(bis(4-fluorophenyl)methyl)piperazine (for **3d**) / 2-(3,4-dimethoxyphenyl)-*N*-methylethan-1-amine (for **3e**), $CuSO_4$, HCHO, EtOH/$H_2O$, reflux, 24 h; iv) $NaN_3$, DMSO, r.t., 24 h; v) 1-(bis(4-fluorophenyl)methyl)-4-(prop-2-yn-1-yl)piperazine (for **3f**) / *N*-(3,4-dimethoxyphenethyl)-N-methylprop-2-yn-1-amine (for **3g**), $CuSO_4$, Na-ascorbate, DMSO, 80-90 °C, 24 h.

*2.2 Biological evaluation*

*2.2.1 Effect on cell proliferation*

HL60 cell line and its MDR counterpart HL60R were treated with the newly synthetized polycyclic derivatives and lead compound **2** for 24 hours. Compound **1** was not used as reference for the evaluation of the antitumor effect, since it did not show cytotoxicity when tested alone on leukemic cells. [13]. Therefore, the intrinsic antitumor activity of the molecules under test was compared to that of compound **2**, to date the only polycyclic derivative with dual reverting and anticancer activity.

The viability assay revealed that all compounds were able to halve the cell population in sensitive HL60 cells, with $IC_{50}$ values ranging from 4.8 to 22 μM (Table 1). Some derivatives were even more active than lead compound **2**. In particular, **3c** resulted the most potent of the series, followed by **3f**, **3g** and **3b**, being active at concentrations lower than 10 μM. Derivatives **3a**, **3d,** and **3e** only showed a moderate activity. The results obtained on HL60R cells seem to follow the same trend, although significant differences in terms of potency can be found. Compound **3c** remained the most active, however it proved to be five-fold more antiproliferative on resistant cells with respect to sensitive ones, thus showing a moderate CS. The peculiar ability to selectively hit resistant cells

could represent an additional tool to counteract MDR phenomenon in cancer cells. Compounds **3a, 3d** and **3e** were the least active of the series again, as concentrations above 20 μM were required to reduce MDR cells viability. In particular, the $IC_{50}$ value of **3d** was above 100 μM, and consequently it was not used for further antitumor analysis. Regarding **3b**, **3f**, and **3g**, a similar and significant effectiveness was observed. All three compounds were able to reduce the resistant cell population by 50% when used at concentrations around 10 μM, as in sensitive cells. From a structural point of view, some considerations can be drawn: compounds **3a-c**, bearing a 1,2,3-triazole ring in the side chain, proved to be more potent than both the reference **2** and the pent-3-ynyl-based derivatives **3d** and **3e**, and the methoxy groups appeared of key relevance for obtaining good potency (**3b** and **3c** *vs* **3a**). Moreover, for a good antiproliferative activity, the possibility for the nitrogen atom in the side chain to be protonated seemed not to be significant, being compounds **3b** and especially **3c** the most active, though the least basic of the series. When a protonable nitrogen was present, as in compounds **3f** and **3g**, the nature and the size of the amine did not appear to influence activity. The length of the chain also seemed not to be important for activity, showing compounds **3b** and **3g** different chain length and different basicity, but similar potency on both cell lines. Surprisingly, when comparing compounds **3b** and **3c**, the influence of the side chain length could be appreciated, being the two-methylene-based **3c** twice as potent on sensitive cells and seven-fold more potent on their MDR counterpart with respect to **3b** with a one-methylene linker.

**Table 1.** Cell viability for HL60 and HL60R cell lines following treatment with compounds **2**, **3a-g**.

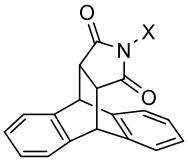

| Compound | X | R | $R_1$ | $IC_{50}$ (μM) [a] [Int. confidence 95%] | |
|---|---|---|---|---|---|
| | | | | HL60 | HL60R |
| **2** | 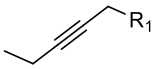 | - | B | **13.0** [10:15] | **3.3** [1.9:5.7] |
| **3a** | 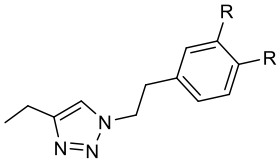 | H | - | **14.7** [12:17] | **24.0** [19.7:29.5] |
| **3b** | 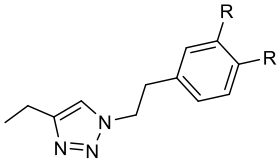 | $OCH_3$ | - | **8.6** [6.4:11.6] | **7.2** [5.9:8.9] |
| **3c** | 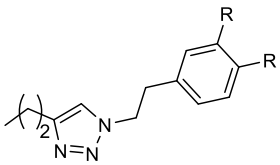 | $OCH_3$ | - | **4.8** [3.8:5.9] | **1.0** [0.75:1.3] |
| **3d** |  | - | A | **22.0** [16:28] | >100 |
| **3e** |  | - | B | **10.8** [8.9:13] | **22.0** [6.4:76] |

| | | | | | |
|---|---|---|---|---|---|
| **3f** | 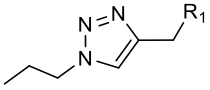 | - | A | **7.4** [6.5:8.4] | **11.9** [8:17] |
| **3g** | 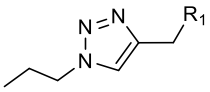 | - | B | **8.2** [6.6:10.2] | **7.6** [7:8.4] |

[a]Half-maximal inhibitory concentration ($IC_{50}$) was determined from the dose-response curve by MTT assay (95% confidence interval); three independent experiments were performed with four wells per each treatment preparation.

*2.2.2 Effect on cell cycle*

The effects of the newly synthetized polycyclic derivatives on cell cycle progression were also assessed by flow cytometry to further evaluate their antitumor profile. After 24 h of exposure, cell cycle modifications were observed in both sensitive and MDR leukemic cells. In particular, the lead compound **2** determined an increase in G1 (from 34 to 44 %) and a relative decrease in S phase (from 53 to 43 %), while G2/M phase remained unchanged in HL60 cells. Except for compounds **3a** e **3g**, which did not induce any effect on cell cycle, all tested molecules determined a DNA profile similar to that of compound **2** (Figure 3a).

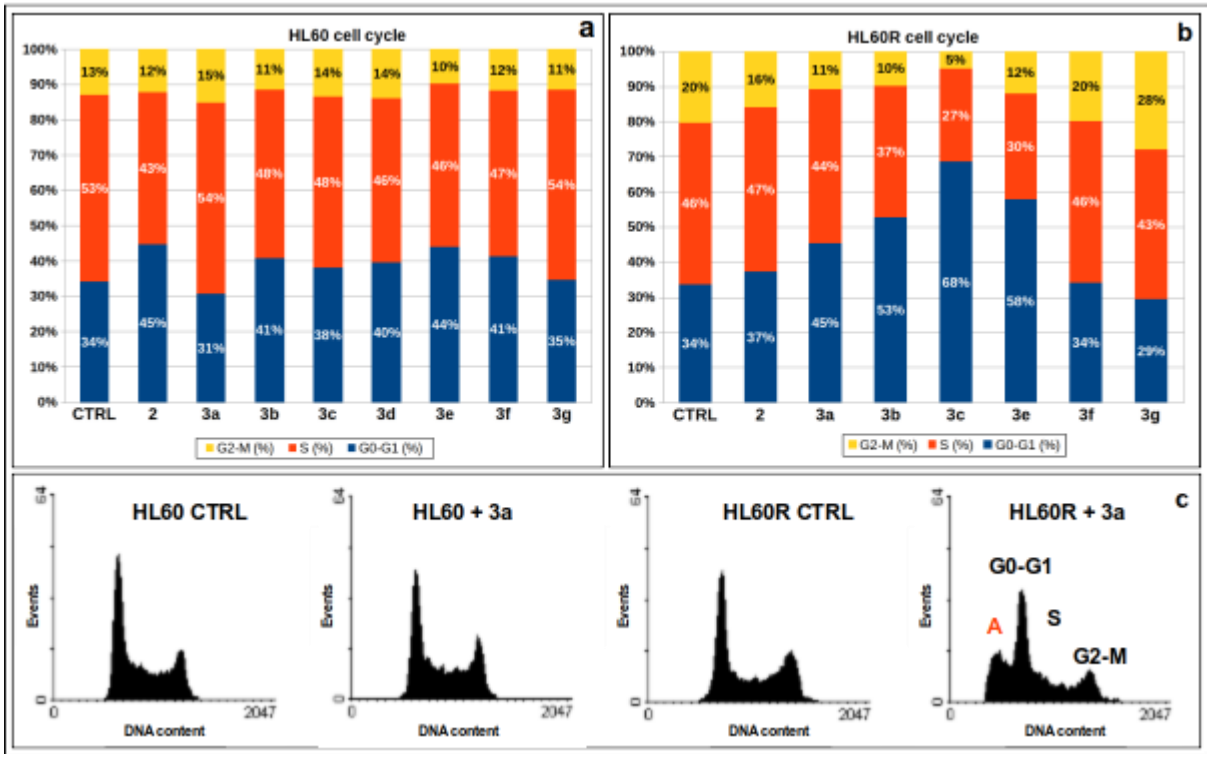


**Figure 3.** Cell cycle analysis of HL60 cells (a) and HL60R (b) after treatment with $IC_{50}$ concentrations of polycyclic derivatives for 24 h. Panel (c) shows DNA profiles of sensitive and resistant cells after treatment with compound **3a**: a marked apoptosis (red A) is induced only n MDR cells .

Interestingly, the treatment of MDR cells produced more striking and differentiated effects on cell cycle. Generally, the new compounds induced a marked block in G1 phase, unlike the ineffective lead compound **2** (figure 3b). The most significant effect was detected with compound **3c** followed by **3e**, **3b** and **3a**, being G0/G1 cell percentages 68 %, 58 %, 53 % and 45 %, respectively, *versus* 34 % of the control samples. Among these active compounds, **3a** was able to induce apoptosis, since a considerable number of cells showing a reduced content of DNA appeared after treatment, and a consistent sub-$G_1$ peak was visible in the cytometric analysis (figure 3c, red A). Although **3a** required a higher concentration to affect MDR cells proliferation with respect to sensitive cells, its

effect is clear and unequivocal. It can be supposed that here CS is achieved not in terms of concentration ($IC_{50}$ is higher) but in terms of desirable cytotoxic effect. Once the sufficient concentration is reached, **3a** triggers apoptosis, probably recognizing specific targets in the multidrug phenotype. Finally, **3f** did not alter cell cycle profile, while **3g** induced a modest accumulation of cells in G2/M phase (figure 3b). Since the MTT assay demonstrated that all members of the series were able to reduce cell population, the absence of significant perturbations on cell cycle for some of them suggests different mechanisms and/or a different timing of action.

Recently, metabolic alterations associated with the MDR phenotype in cancer and their intercellular transfer mediated by extracellular vesicles have been identified [25]. The most pronounced activity of some polycyclic derivatives against MDR cells could be explained by the interaction with metabolites or small lipid structures, specifically present in the extracellular medium of resistant cells. It is reasonable to hypothesize that increased bioavailability or more efficient delivery are the reasons for the overcoming of drug resistance and potentiation of the effects on cell.

*2.2.3 Effects on multidrug resistance*

The revertant activity of the new polycyclic derivatives was evaluated on MDR leukemic cells by flow cytometry, measuring the intracellular accumulation of the typical P-gp substrate Rhodamine 123 (R123), a lipophilic cation whose levels can be detected in intact cells thanks to its intrinsic fluorescence. Thus, R123 accumulation in (or efflux from) cells is useful to reveal the P-gp-dependent transport activity [26]. High intracellular R123 levels can be interpreted as low P-gp activity, and thus P-gp inhibitors would be expected to lead to enhanced accumulation of the dye in MDR cells, as they interfere with its extrusion.

The results, depicted in Figure 4a, show that all tested compounds determined an inhibition of the P-gp efflux pump, even though to different extent. In particular, **3d, 3e**, and **3f** exhibited a remarkable activity, significantly superior to the prototype MDR reversal agent verapamil and higher than, or comparable to, that of lead compounds **1** and **2**, restoring the intracellular levels of fluorescence up to those of sensitive cells. Compound **3c** also showed a significant effect, while compounds **3a**, **3b** and **3g** exhibited lower activity, still comparable to that of verapamil.

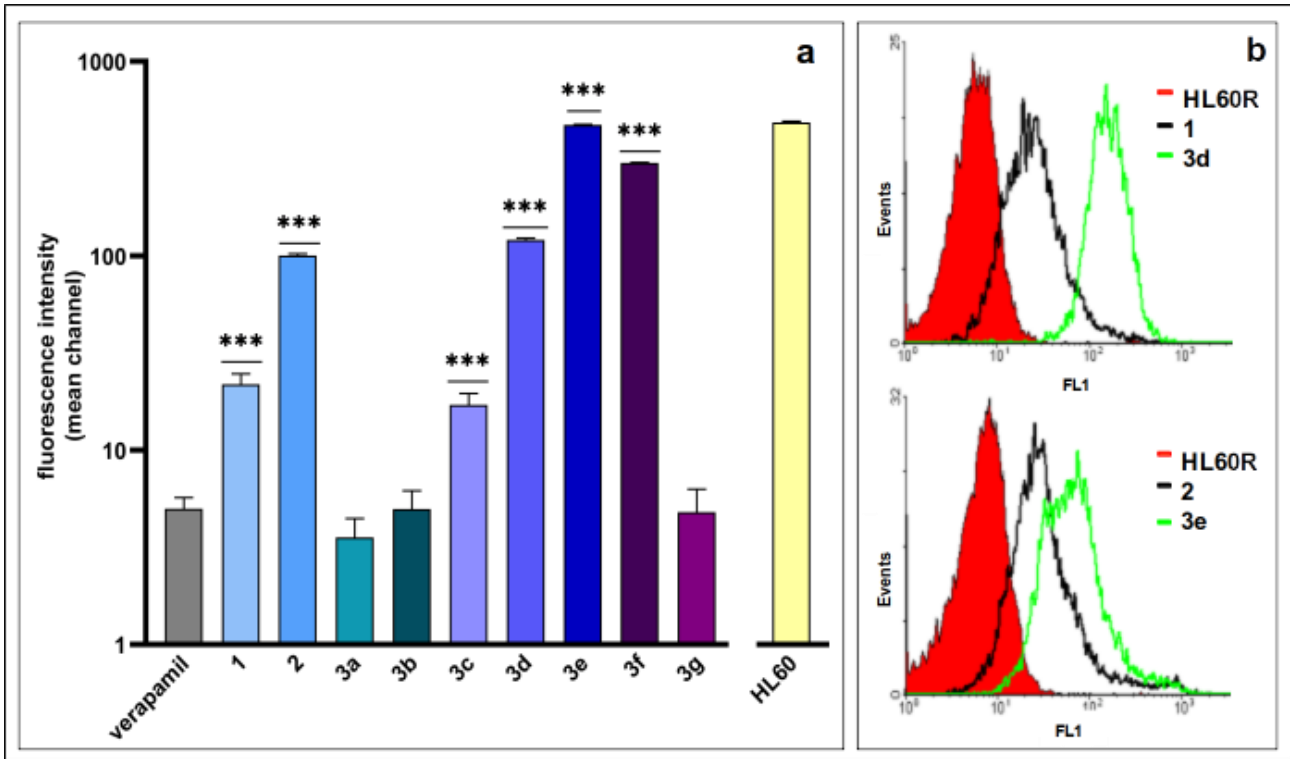


**Figure 4. (a**) Revertant activity of compounds **1**, **2** and **3a-g** (10 μM) on HL60R cells evaluated as Rhodamine123 uptake; the fluorescence of HL60 cells are reported for comparison. Bars represent mean ± SD from three independent experiments. Statistics is performed by one-way ANOVA test versus verapamil treated cells (*** $p<0.001$). (**b**) Overlay plot of the Rhodamine 123 fluorescence distributions in control and in HL60R treated with compound **1** and **3d** (upper) and with compound **2** and **3e** (lower).

From a structural point of view, it is evident that all compounds showed a potent reverting profile, confirming the pivotal role of the polycyclic scaffold and the properly selected amino group. In a SAR perspective, the MDR reverting activity of the new compounds seems to be in line with previously reported data. The overall lipophilicity of the molecules (miLogP ranging from 3.35 for **3b** to 6.63 for **3d**, with an average of 4.4 [27]) and the presence of aromatic rings, H-bond donor groups, and a protonable nitrogen substantially contribute to the remarkable potency. With respect to the previously reported lead molecules **1** and **2**, in the new series the elongation of the side chain, as in compounds **3d** and **3e**, led to a slight increase in flexibility and lipophilicity, likely responsible for a corresponding increase in reverting potential. This effect is depicted in figure 4b, where a substantial increase in fluorescence can be observed going from **1** and **2** to **3d** and **3e**, respectively.

According to the results reported for previous series,[12,13,18] the *N*-methyl-omoveratrylamine amino group (side function B), present in the prototype verapamil, greatly contributed to MDR reverting activity when inserted in a linear side chain, as in compound **3e**, the most potent of this series. Interestingly, compound **3g**, bearing a triazole ring instead of the triple bond, showed a marked decrease in potency, despite the presence of the same terminal amino function. This behavior could be related to a corresponding decrease in lipophilicity, showing compound **3e** a much higher miLogP (4.69) with respect to **3g** (3.38). A different trend can be observed going from compound **1** to **3d** and **3f**. Here, the introduction of the triazole moiety in the side chain (**3f**) elicited an increase in potency, leading to speculate a more favorable binding network for the piperazine-based amino group (side function A). Notably, compounds **3d** and **3f** showed similar and very high logP values (miLogP 6.63 for **3d** and 5.32 for **3f**), that could positively contribute to their ability to bind P-gp within the lipid bilayer.

Surprisingly, compound **3c**, devoid of the protonable nitrogen atom, still retained appreciable activity, much higher than verapamil. In this respect, a positive role of a longer spacer between the triazole and the polycyclic core should be noticed, being **3c** (two-methylene units) considerably more active than the shorter (one-methylene) **3b**, despite a similar miLogP value. Finally, a favorable contribution to activity can be attributed to the methoxy groups, being compound **3a** the least active of the series, though still comparable to verapamil.

Notably, as regards the mechanism of action of these revertant agents, the compounds cannot be considered substrates of the efflux protein, as their administration to HL60R cells did not induce ATP consumption (see Figure S1, Supplementary Material). This could probably be due to the interaction with a different binding site on P-gp, compared to substrates of the efflux protein, as postulated by computational studies that indicated a different docking pose for these molecules.

*2.3 Docking studies*

Docking studies were performed to investigate the interaction mode of the new compounds in the P-gp binding pocket and to explain their *in vitro* inhibitory activity. For this purpose, a docking simulation was used to predict the correct binding pose of ligands and their interaction network. Molecular docking studies were performed into the 3D crystal of human P-gp (PDB code 6FN1) and the binding region was identified on the same inhibitor binding region in complex with 6FN1. First, a blind docking was carried out, where all ligands were free to bind to the whole protein surface, in order to evaluate a potential binding region for the compounds, and as second step a rational docking was carried out to obtain the final docked pose. As a results of docking simulations, all compounds were seen to share a known P-gp binding region (Figure 5) [28-30].

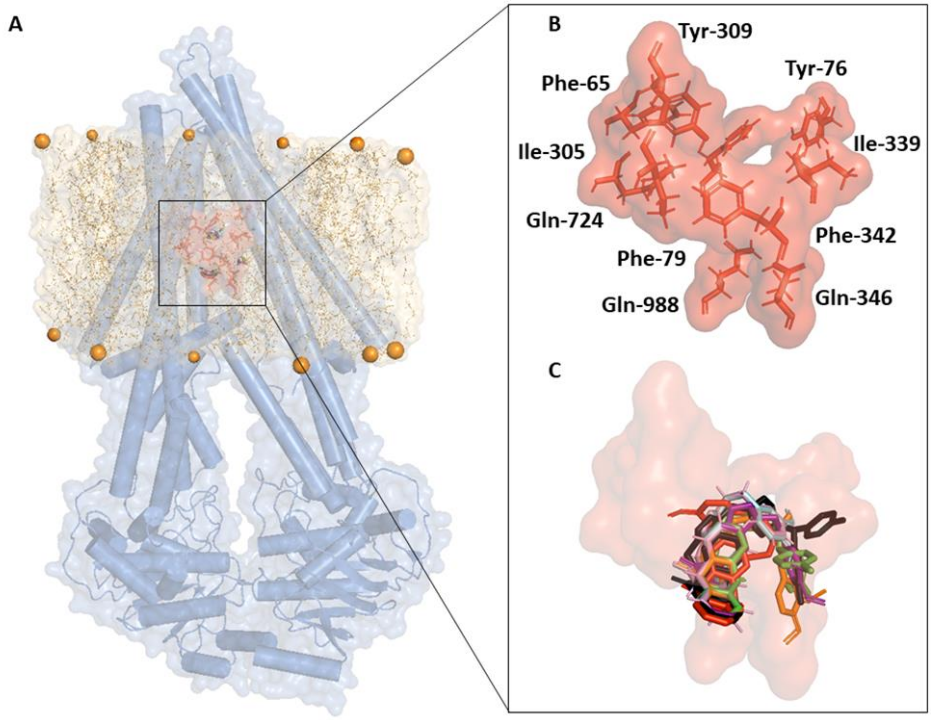


**Figure 5.** 3D representation of human P-gp inside the lipid bilayer in complex with its inhibitors. A) Human P-gp protein is shown as blue cartoon/surface, while the bilayer is reported in light orange stick/surface, the orange spheres representing the hydrophilic heads. In the box are reported all compounds (coloured sticks) located inside the P-gp binding pocket (red stick/surface). B) Enlarged of binding pocket residues and C) the docked poses of ligands within the binding site.

Docking scores revealed that compounds **3f** (-109.1 Kcal/mol), **3e** (-104.7 Kcal/mol) and **3d** (-96.3 Kcal/mol) showed the highest thermodynamics affinity for the target, while **3c** (-83.5 Kcal/mol), **3g** (-83.2 Kcal/mol), **3b** (-79.2 Kcal/mol) and **3a** (-74.5 Kcal/mol) exhibited a lower binding energy, reflecting experimental evidences. To dissect further insights about P-gp/ligand binding, the interaction network of all systems was analysed, performing an energy decomposition for each residue involved in Van Der Waals interactions and hydrogen bonds with the compound (Figure 6).

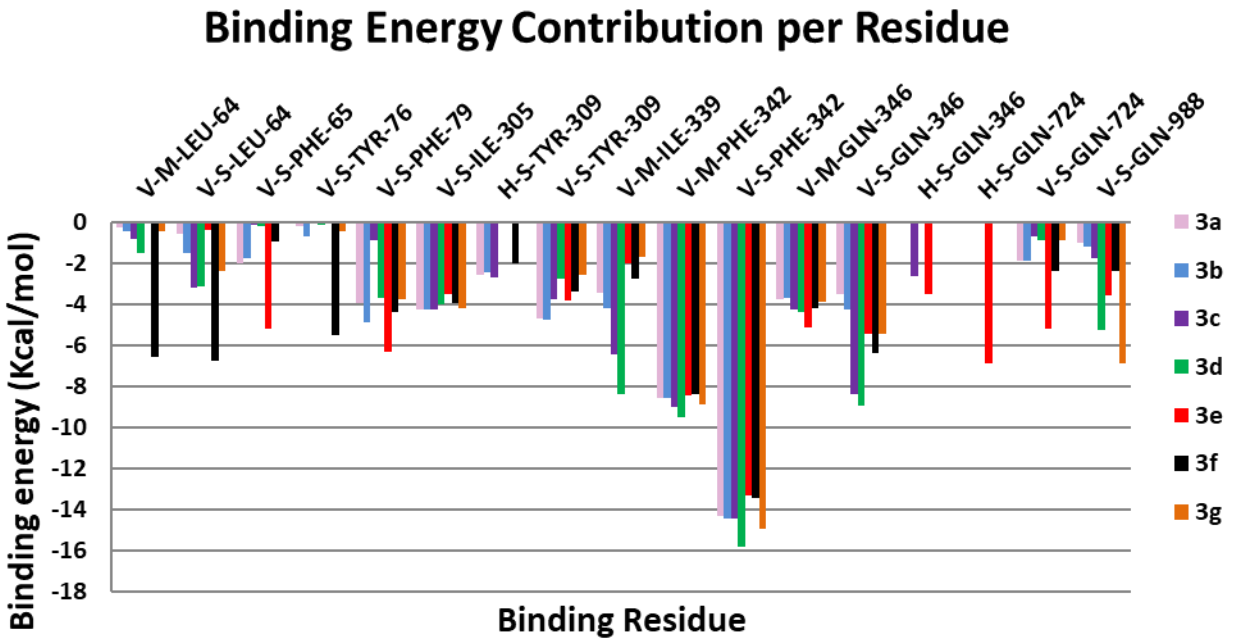


**Figure 6.** Binding Energy Contribution per Residue of human P-gp on each compound. On y and x axis are reported the energy contribution per residue (Kcal/mol) and the binding residue, respectively. The binding residue/compound interaction is indicated as H-S (Hydrogen bond-Side chain), V-M (Van Der Waals interaction-Main chain) and V-S (Van Der Waals interaction-Side chain).

Analysis of the obtained interaction profile showed how each compound formed different interactions with residues that are generally known to be involved in P-gp/inhibitors interaction [31]. All ligands formed an interesting hydrophobic network with human P-gp binding pocket, but not all compounds, likely due to the different atomic composition and their chemical structure, were involved in the same interaction network. Indeed, **3d**, **3e** and **3f**, differently from other ligands, presented interactions with high energy and specific bond types. In detail, **3d** formed a strong Van Der Waals interaction between

the fluorobenzene ring and Ile-339 β-carbon and a halogen bond with the fluorine of the fluorobenzene ring and the γ-oxygen of Ser-343; **3f** exhibited hydrophobic interactions with high energy between the fluorobenzene ring and γ and δ2 carbons of Leu-64 and with the ζ1-carbon of the Tyr-76; finally, **3e** formed strong hydrophobic interactions among the 3,4-dimethoxybenzyl ring and ϵ2-carbon of Phe-65 and the δ2-carbon of Phe-79 and a hydrogen bond between the para-methoxy group of the 3,4-dimethoxybenzyl ring and the ϵ2-nitrogen of the amide group of Gln-724. Interestingly, **3e** was the only compound able to form a strong hydrogen bond with this residue, and a previous work [32] showed that Gln-724 was a key residue both in the binding of P-gp inhibitors and in protein biological function. Such computational evidence would thus explain the highest experimental inhibitory activity of **3e** of all compounds, highlighting the importance of Gln-724-**3e** hydrogen bond. Another interesting result is the ability of each compound to form a strong π-stacking with the aromatic ring of Phe-342, revealing a potential key role for this residue in the binding and mechanism of action of P-gp inhibitors.

Docking simulations and interaction network analyses were also performed for verapamil to clarify the different mechanisms of action between our revertant agents and the substrates of the efflux protein, a well-known P-gp substrate. These computational studies demonstrated that verapamil would bind to the P-gp on a different or partially overlapping site compared to our compounds, with a different interaction network (Figure S2, Supplementary material), as suggested in other previous works [33]. In particular, Ahmad R. Safa, [34 ] showed that verapamil binding site on P-gp could have several points involved in hydrophobic and H-bonds interactions, and different binding modes, conferring a different mechanism of action on the protein. Such evidences would explain the different mechanisms of action between verapamil and our compounds. Indeed, from *in silico* results, both

potential critical binding residues for the inhibition of human P-gp and key interactions for the mechanism of action of our ligands were identified (Figure 7).

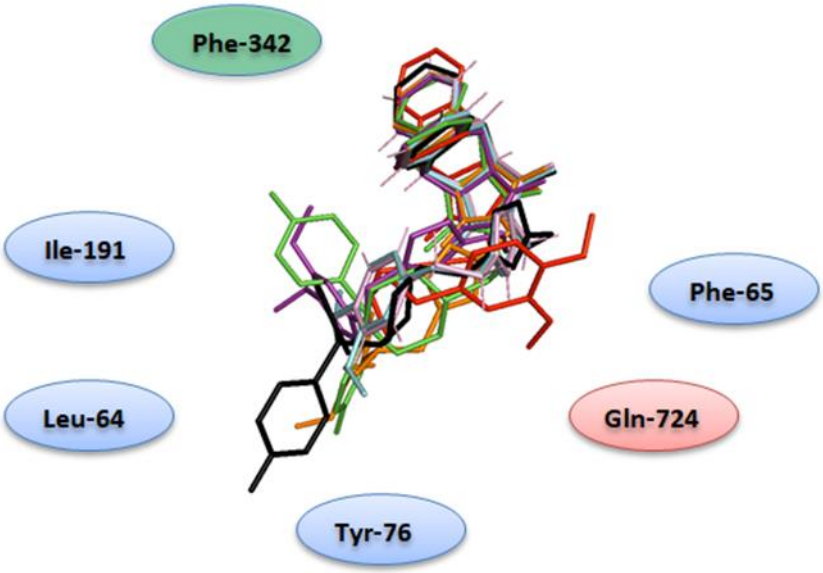


**Figure 7.** Key elements for compounds activity at the human P-gp protein. The compounds are shown as coloured sticks (as indicated in fig. 5). In red, blue and green circles are reported the key binding residues involved in hydrogen bonds, hydrophobic and π-stacking interactions respectively.

## 3. Conclusions

In this study, the effects of the modification of the spacer and the nitrogen-containing group of our previously reported potent modulators of MDR, have been investigated. Primarily, these results confirm that the polycyclic core of these compounds represents a valuable privileged structure in medicinal chemistry.

A further increase in reverting potency was observed, in particular when the side chain was elongated by one methylene unit, *i.e.* from the previously employed but-2-ynyl to a pent-3-ynyl-

amino moiety, as in **3d** and **3e**. Interestingly, the triazole ring, introduced *via* the click chemistry approach, induced a different behaviour depending on the nature of the terminal amino group. Indeed, compound **3f**, carrying side chain A, was much more potent than **3g**, bearing the amino-terminal group B shared by both verapamil and **3e**, the most active of the series. The reduced MDR reverting activity of **3g** could be related to a lower lipophilicity and to a different binding network with P-gp. Notably, the inclusion of the *N*-methylamino group of function B in the 1,2,3-triazole ring, as in compound **3c**, seemed to be particularly beneficial for activity. The docking results supported the data obtained by the biological tests, since all compounds are able to dock into P-gp binding site with a good thermodynamic affinity. The appreciable activity of compounds **3d**, **3e** and **3f** could be related to the specific bonds (and their greater strength) that these molecules are able to establish with the protein. In this respect, **3e** proved to be the only compound of the series capable of engaging Gln724, deemed as a key residue for P-gp inhibitors binding and for protein functioning.

Looking at the whole biological profile of the new compounds, beyond the optimization of the revertant activity, multifaceted active compounds were obtained. Generally, all of them showed a dual activity, inducing both revertant and antitumor effects on leukemic cells, as the lead compound **2**. Intriguingly **3a**, while showing a weak reverting potential, proved to induce massive apoptosis on resistant cells, an effect that opens new perspectives in the synthesis of more specific and targeted agents against no longer sensitive cancer cells. Furthermore, **3c** could be regarded as a "triple-target" agent, endowed with an appreciable reverting potency, also showing a considerable antiproliferative activity and a CS profile. This capability, offering a significant contribute at counteracting MDR phenomenon, pinpoints this compound as a promising anticancer agent, worth to be further explored. Finally, many intriguing questions arise: are the molecular targets and the

transduction pathways involved in antitumor activity the same in sensitive and in MDR cells? Is the increased activity in resistant cells given by the overexpression of the target or by the different metabolites present in the cellular environment? An in depth study of compound **3c**, evaluating its effect on gene expression and/or metabolome in different resistant cell lines could try to give a possible answer to these questions.

## 4. Experimental protocols

### *4.1. Chemistry.*

*4.1.1. General Methods*. Starting materials, unless otherwise specified, were used as high-grade purity commercial products. Solvents were of analytical grade. Reaction progress was followed by thin layer chromatography (TLC) on precoated silica gel plates (Merck Silica Gel 60 F254) and then visualized with a UV254 lamplight. Chromatographic separations were performed on silica gel columns by flash method (Kieselgel 40, 0.040-0.063 mm, Merck). Melting points were determined in open glass capillaries, using a Büchi apparatus and are uncorrected. $^{1}$H NMR and $^{13}$C NMR spectra were recorded on a Varian Gemini spectrometer 400 MHz and 101 MHz, respectively, in $CDCl_3$ solutions unless otherwise indicated, and chemical shifts (δ) were reported as parts per million (ppm) values relative to tetramethylsilane (TMS) as internal standard; coupling constants (*J*) are reported in Hertz (Hz). Standard abbreviations indicating spin multiplicities are given as follow: s (singlet), d (doublet), t (triplet), br (broad), q (quartet) or m (multiplet). Mass spectra were recorded on Waters ZQ 4000 apparatus operating in electrospray mode (ES). Chemical purities of tested compounds were determined by elemental analysis (C, H, N) and were within ± 0.4 % of the

theoretical values. Compounds were named relying on the naming algorithm developed by CambridgeSoft Corporation and used in ChemDraw Professional 15.0.

*4.1.1.1. 13-(but-3-yn-1-yl)-9,10-dihydro-9,10-[3,4]epipyrroloanthracene-12,14-dione (6)*

Potassium *tert*-butoxide (0.4 g, 3.6 mmol, 1.3 eq) was added to a suspension of **4** [23] (0.75 g, 2.6 mmol, 1 eq) in DMSO (15 mL) and the mixture was stirred at rt for 30 min. The obtained solution was then added dropwise to a solution of 4-bromobut-1-yne (0.36 g, 2.6 mmol, 1 eq) in DMSO, stirred at room temperature for 5 h and then poured into ice. The solid formed was collected by filtration, and then purified by flash column chromatography (toluene/acetone 4:1), to yield 0.45 g of **6** (47 %) as a white solid. Mp 189-191 °C. $^1$H NMR δ: 1.51-1.55 (m, 2H), 1.88 (t, *J* = 2.4 Hz, 1H), 3.18 (s, 2H), 3.20-3.27 (m, 2H), 4.78 (s, 2H), 7.11-7.17 (m, 4H, Ar), 7.18-7.20 (m, 2H, Ar), 7.34-7.37 (m, 2H, Ar).

*4.1.1.2 13-(2-bromoethyl)-9,10-dihydro-9,10-[3,4]epipyrroloanthracene-12,14-dione (7)*

Compound **7** was obtained following the previous described procedure, using 4 and 1,2-dibromoethane as starting materials. After filtration, the collected solid was purified by crystallization (ethyl acetate), to yield 0.96 g of **7** (89 %, white crystals). Mp 178-180 °C. $^1$H NMR δ: 2.53 (t, *J* = 7.6 Hz, 2H), 3.23 (s, 2H), 3.47 (t, *J* = 7.6 Hz, 2H), 4.80 (s, 2H), 7.14-7.20 (m, 4H, Ar), 7.26-7.28 (m, 2H, Ar), 7.37-7.39 (m, 2H, Ar).

*4.1.1.3. 13-(2-azidoethyl)-9,10-dihydro-9,10-[3,4]epipyrroloanthracene-12,14-dione (8)*

To a solution of $NaN_3$ (0.08 g, 1.2 mmol, 1.4 eq) in DMSO (20 mL), 0.32 g (0.84 mmol, 1 eq) of **7** were added and the mixture was stirred at rt for 24 h, heated at 70-80 °C for further 3 h and poured into ice. After extraction with ethyl acetate (3 x 50 mL), the organic layer was washed with brine, dried over anhydrous $Na_2SO_4$ and concentrated under reduced pressure, to give 0.26 g (90 %) of **8**

as white solid, which was used for the subsequent step without pufication. Mp 128-132 °C. $^{1}$H NMR δ: 2.72 (t, *J* = 6.8 Hz, 2H), 3.23 (s, 2H), 3.27 (t, *J* = 6.8 Hz, 2H), 4.79 (s, 2H), 7.16-7.19 (m, 4H, Ar), 7.26-7.29 (m, 2H, Ar), 7.37-7.39 (m, 2H, Ar).

*4.1.1.4 General method for the copper catalyzed azyde-alkyne cycloaddiction*

To a solution of the alkyne (1 eq) in DMSO (15 mL), the selected azyde (1.3 eq) and triethylamine (4.7 eq) were added. A solution of $CuSO_4$ (0.1 eq) and Na-ascorbate (0.5 eq) in $H_2O$ (2 mL) was prepared and promptly added to the reaction mixture, that was heated at 80-90 °C with stirring for 24 h and then poured into ice. The solid formed was filtered and dissolved in ethyl acetate; the solution washed with $H_2O$, dried over $Na_2SO_4$, and the solvent was evaporated to dryness. The obtained crude was purified by flash chromatography or by crystallization.

*4.1.1.5. 13-((1-phenethyl-1H-1,2,3-triazol-4-yl)methyl)-9,10-dihydro-9,10-[3,4]epipyrroloanthracene-12,14-dione (3a)*

Starting from **5** [23] and (2-azidoethyl)benzene, 0.18 g (38 %) of **3a** were obtained. Purification by flash chromatography (toluene/acetone 4.5:0.5). Mp 204-206 °C. $^{1}$H NMR δ: 3.15 (t, *J* = 7.6 Hz, 2H), 3.25 (s, 2H), 4.42-4.50 (m, 4H), 4.79 (s, 2H), 6.36 (s, 1H), 7.00-7.02 (m, 2H, Ar), 7.10-7.12 (d, *J* = 7.2 Hz, 2H, Ar), 7.16-7.21 (m, 4H, Ar), 7.31-7.38 (m, 5H, Ar). $^{13}$C NMR δ: 175.9, 141.4, 138.9, 128.9, 128.6, 127.1, 126.8, 126.6, 125.0, 124.2, 122.0, 51.4, 46.8, 45.3, 36.7, 33.8. ES-MS: m/z 483 ($M+Na^{+}$).

*4.1.1.6. 13-((1-(3,4-dimethoxyphenethyl)-1H-1,2,3-triazol-4-yl)methyl)-9,10-dihydro-9,10-[3,4]epipyrroloanthracene-12,14-dione (3b)*

Starting from **5** [23] and 4-(2-azidoethyl)-1,2-dimethoxybenzene [22], 0.05 g (13 %) of **3b** were obtained. Purified by flash chromatography (toluene/acetone 4:1). Mp 214-216 °C (toluene). $^{1}$H

NMR δ: 3.09 (t, *J* = 7.2 Hz, 2H), 3.24 (s, 2H), 3.81 (s, 3H), 3.87 (s, 3H), 4.37-4.41 (m, 4H), 4.77 (s, 2H), 6.35 (s, 1H), 6.48 (d, *J* = 1.6 Hz, 1H, Ar), 6.65 (dd, *J* = 2.0 and 8.2 Hz, 1H, Ar), 6.81 (d, *J* = 8.4 Hz, 1H, Ar), 6.97-6.99 (m, 2H, Ar), 7.15-7.20 (m, 4H, Ar), 7.35-7.37 (m, 2H, Ar). $^{13}$C NMR δ: 175.9, 147.6, 146.8, 141.4, 138.9, 128.6, 127.1, 126.6, 124.2, 122.0, 112.8, 112.3, 51.4, 50.6, 46.8, 45.4, 36.7, 33.7. ES-MS: m/z 543 ($M+Na^+$).

*4.1.1.7. 13-(2-(1-(3,4-dimethoxyphenethyl)-1H-1,2,3-triazol-4-yl)ethyl)-9,10-dihydro-9,10-[3,4]epipyrroloanthracene-12,14-dione (3c)*

Starting from **6** and 4-(2-azidoethyl)-1,2-dimethoxybenzene [24], 0.06 g of **3c** (25 %) were obtained as colourless oil. Purified by flash chromatography (toluene/acetone 4:1). $^1$H NMR δ: 2.11 (t, *J* = 8.0 Hz, 2H), 3.09 (t, *J* = 7.2 Hz, 2H), 3.19 (s, 2H), 3.32 (t, *J* = 8.0 Hz, 2H), 3.79 (s, 3H), 3.84 (s, 3H), 4.46 (t, *J* = 7.2 Hz, 2H), 4.78 (s, 2H), 6.50 (d, *J* = 1.2 Hz, 1H), 6.63 (dd, *J* = 1.6 and 7.2 Hz, 1H, Ar), 6.78 (d, *J* = 8.2 Hz, 1H, Ar), 6.99 (s, 1H, Ar), 7.08-7.10 (m, 2H, Ar), 7.15-7.17 (m, 2H, Ar), 7.20-7.26 (m, 2H, Ar), 7.36-7.38 (m, 2H, Ar). $^{13}$C NMR δ: 176.7, 149.1, 148.1, 143.8, 141.5, 138.8, 129.7, 127.1, 126.9, 125.1, 124.3, 121.7, 120.8, 111.9, 111.5, 56.0, 55.9, 51.8, 46.8, 45.7, 37.7, 36.5, 29.4, 23.2. ES-MS: m/z 557 ($M+Na^+$).

*4.1.1.8. 13-(2-(4-((4-(bis(4-fluorophenyl)methyl)piperazin-1-yl)methyl)-1H-1,2,3-triazol-1-yl)ethyl)-9,10-dihydro-9,10-[3,4]epipyrroloanthracene-12,14-dione (3f)*

Starting from 1-(bis(4-fluorophenyl)methyl)-4-(prop-2-yn-1-yl)piperazine and **8**, 0.14 g of **3f** (35 %) were obtained. Purified by flash chromatography (toluene/acetone 4:1). Mp 233-237 °C $^1$H NMR δ: 2.35-2.40 (m, 4H), 2.49-2.52 (m, 4H), 3.22 (s, 2H), 3.50 (t, *J* = 7.6 Hz, 2H), 3.64 (s, 2H), 3.68 (t, *J* = 7.6 Hz, 2H), 4.22 (s, 1H), 4.77 (s, 2H), 6.95 (t, *J* = 8.8 Hz, 4H, Ar), 7.11-7.13 (m, 2H, Ar), 7.16-7.18 (m, 2H, Ar), 7.26-7.28 (m, 2H, Ar), 7.30-7.36 (m, 2H, Ar), 7.34-7.36 (m, 5H, Ar).

$^{13}$C NMR δ: 176.3, 163.1, 160.7, 141.2, 138.9, 138.3, 129.4, 129.3, 127.2, 127.0, 125.2, 124.4, 122.8, 115.5, 115.3, 74.5, 53.1, 51.6, 46.9, 46.0, 45.6, 37.6 ES-MS: *m/z* 671 ($M+H^+$), 693 ($M+Na^+$).

*4.1.1.9.. 13-(2-(4-(((3,4-dimethoxyphenethyl)(methyl)amino)methyl)-1H-1,2,3-triazol-1-yl)ethyl)-9,10-dihydro-9,10-[3,4]epipyrroloanthracene-12,14-dione (3g)*

Starting from *N*-(3,4-dimethoxyphenethyl)-N-methylprop-2-yn-1-amine and **8**, 0.06 g of **3g** were obtained (22 %), as colourless oil. Purified by flash chromatography (toluene/acetone 4:1, and then DCM/acetone 1:1). $^1$H NMR δ: 2.33 (s, 3H), 2.63 (t, *J* = 7.6 Hz, 2H), 2.75-2.78 (m, 2H), 3.23 (s, 2H), 3.50 (t, *J* = 7.6 Hz, 2H), 3.69-3.72 (m, 4H), 3.85 (s, 3H), 3.86 (s, 3H), 4.77 (s, 2H), 6.73 (d, *J* = 7.2 Hz, 2H, Ar), 6.79 (d, *J* = 8.4 Hz, 1H, Ar), 7.12-7.14 (m, 2H, arom), 7.17-7.21 (m, 2H, Ar), 7.22 (s, 1H, Ar), 7.26-7.28 (m, 2H, Ar), 7.36-7.38 (m, 2H, Ar). $^{13}$C NMR δ: 176.3, 148.9, 147.4, 145.5, 141.2, 138.9, 133.1, 127.2, 127.0, 125.2, 124.4, 122.7, 120.7, 112.3, 111.4, 59.0, 56.0, 55.9, 52.4, 46.9, 46.1, 45.6, 42.2, 37.6, 33.6. ES-MS: *m/z* 578 ($M+H^+$), 600 ($M+Na^+$).

*4.1.1.10. General method for the Mannich reaction.*

To a solution of compound **6** (0.3 g, 1.0 mmol) in EtOH/$H_2O$ (1:1, 15 mL) a mixture of the selected amine (1.0 mmol, 1 eq), HCHO (0.2 mL) and $CuSO_4$ (0.01 g) was added and the resulting suspension was heated under reflux for 24 h. After cooling, $NH_4OH$ (10 mL) was slowly added and the obtained mixture was extracted with diethyl ether (3 x 20 mL); the combined organic layers were dried over $Na_2SO_4$ and evaporated to dryness. The crude was purified by flash chromatography.

*4.1.1.11. 13-(5-(4-(bis(4-fluorophenyl)methyl)piperazin-1-yl)pent-3-yn-1-yl)-9,10-dihydro-9,10-[3,4]epipyrroloanthracene-12,14-dione (3d)*

Starting from **6** and 1-(bis(4-fluorophenyl)methyl)piperazine, **3d** was obtained (59 %). Mp 195-196 °C (ethanol). $^1$H NMR δ: 1.58-1.61 (m, 2H), 2.34-2.42 (m, 4H), 2.48-2.52 (m, 4H), 3.16 (s, 2H),

3.20-3.25 (m, 4H), 4.23 (s, 1H), 4.82 (s, 2H), 6.90-7.11 (m, 4H, Ar), 7.10-7.18 (m, 4H, Ar), 7.24-7.35 (m, 8H, Ar). $^{13}$C NMR δ: 176.6, 163.3, 160.9, 141.4, 138.3, 129.4, 129.3, 125.2, 124.8, 122.7, 115.5, 115.2, 76.7, 74.5, 73.6, 51.6, 46.9, 46.0, 45.6, 44.6, 37.6, 16.6. ES-MS: *m/z* 650 (M+ $Na^+$).

*4.1.1.12. 13-(5-((3,4-dimethoxyphenethyl)(methyl)amino)pent-3-yn-1-yl)-9,10-dihydro-9,10-[3,4]epipyrroloanthracene-12,14-dione (3e)*

Starting from **6** and 2-(3,4-dimethoxyphenyl)-N-methylethan-1-amine, **3e** was obtained (40 %) as colourless oil. Purified by flash chromatography (toluene/acetone 4:1). $^1$H NMR δ: 1.56 (t, *J* = 7.8 Hz, 2H), 2.29 (s, 3H), 2.56-2.59 (m, 2H), 2.66-2.70 (m, 2H), 3.17 (s, 2H), 3.22 (t, *J* = 8.0 Hz, 2H), 3.27 (s, 2H), 3.85 (s, 3H), 3.88 (s, 3H), 4.77 (s, 2H), 6.72-6.74 (m, 2H, Ar), 6.77-6.80 (m, 1H, Ar), 7.12-7.14 (m, 2H, Ar), 7.16-7.18 (m, 2H, Ar), 7.24-7.25 (m, 2H, Ar), 7.36-7.38 (m, 2H, Ar). $^{13}$C NMR δ: 176.4, 148.8, 147.3, 141.3, 138.6, 132.8, 126.9, 126.7, 124.9, 124.2, 120.4, 112.0, 111.3, 80.8, 76.2, 57.7, 55.9, 55.8, 46.7, 45.8, 45.6, 41.8, 37.1, 33.8, 16.8. ES-MS: *m/z* 535 (M+$H^+$), 557 (M+ $Na^+$).

*4.2. Docking studies*

The starting structure of the P-glycoprotein for docking were taken from the Human P-gp (hP-gp) cryo-EM structure (PDB ID: 6FN1, chains A and B)[29] with a resolution of 3.58 Å in presence of an its inhibitor. To rebuilt missing side chains, PyMOD2.0 [35] was used, finally, the validity of model was evaluated through Ramachandran plot and PROCHECK analyses [36]. To relax energically the structures, each system was inserted inside POPCs 128 (1-palmitoyl-2-oleoyl-glycero-3-phosphocholine) bilayer, solvated with TIP3P water models and neutralized with $Na^+$ ions. The biological systems were built and parameterized (incluse ligands) from CHARMM-GUI platform [37], using CHARMM-36 force field. To fix all bond angles and to minimize steric clashes the systems were subjected to energy minimization , using the steepest descent algorithm, obtaining

the net inter-atomic force for each atom close to zero. P-glycoprotein 3D structure was converted in pdqt format using a MGLTOOLS script [38]. Verapamil 3D structure was downloaded from the pubchem database (Compound CID: 2520) [39] while, our compounds, firstly, were drawn with chemdraw tool and then, all compounds, were converted from the sdf format in pdbqt format with open babel tool [40], adding gasteiger as partial charge. To generate the conformation P-glycoprotein/ligand complexes, a docking simulation was performed with Autodock/VinaXB [41] and the interaction profile was analysed by iGemDock v2.1 [42]. P.L.I.P. software detected the protein/ligand interaction types [43]. PyMOL v2.3 was used as Molecular Graphics System.

*4.3. Biological evaluation.*

*4.3.1 Reagents*

All reagents were from Sigma Aldrich (St. Louis, Mo, USA) if not specifically stated, and were Ultrapure grade.

*4.3.2 Cell culture and treatment*

Human promyelocytic leukemic cell line HL60 was purchased from American Type Culture Collection (ATCC, Manassas, VA) and its MDR subline resistant to doxorubicin (HL60 R) was kindly provided by ML. Dupuis (Istituto Superiore di Sanità, Roma, Italy).

Cells were cultured in RPMI 1640 medium supplemented with 10% foetal bovine serum, L-glutamine and antibiotics. Every ten passages HL60R were treated with doxorubicin 1 μg/mL to maintain drug resistance. All the polycyclic derivatives were dissolved in DMSO and freshly diluted to obtain the requested concentration for the treatments.

*4.3.3 MTT Assay*

Cells were seeded in a 96-well plate at the density of $20 \times 10^4$ cells/mL and exposed for 24 h to increasing concentration of each polycyclic derivative (0.1- 100 μM). For each treatment, the same

concentration of the vehicle DMSO was used as control. 10 µL of tetrazolium salt (5 mg/mL) in PBS were added to culture medium for 4 h. At the end of the incubation, blue-violet formazan salt crystals were formed and dissolved by adding the solution (10% SDS, 0.01 M HCl), then the plates were incubated overnight in humidified atmosphere at 37 °C to ensure complete lysis. The absorbance at 570 nm of the solubilized formazan salt was determined by microplate reader (VICTOR3, Perkin Elmer Life).

The concentrations of derivatives required for 50% inhibition of cell viability ($IC_{50}$) were obtained by dose-response curve interpolation, using Sigma Plot 10.0 software and the $IC_{50}$ values were used for subsequent experiments.

*4.3.4 Cell cycle analysis*

Cell cycle profiles were obtained by flow cytometry. After 24 h of treatment, aliquots of $1 \times 10^6$ cells, in triplicate for each treatment and for the vehicle (DMSO) used as control were washed from growth medium by centrifuging at 240 x *g* for 10 minutes. Next, the pellet was resuspended in 1 ml of a solution containing 0.1% sodium citrate, 0.01% Igepal, 10 µg/ml of RNAse, and 50µg/mL of propidium iodide. After 30 min at 37° C in the dark, the isolated nuclei were analysed by using a Bryte HS flow cytometer (Bio-Rad) equipped with a Xe/Hg lamp and a filter set to obtain an excitation at 488 nm. PI fluorescence was collected on a linear scale at 600 nm, and the DNA distribution was analysed by the ModFit software (Verity, USA)

*4.3.5 Rhodamine 123 uptake assay*

The efflux of rhodamine 123 was performed according to Wieslowa et al.[44]. In brief, the cells were resuspended at the concentrations of $3x10^5$ cells/mL in the culture medium without serum and Phenol Red, and treated with 10 µM of the polycyclic derivatives, the lead compounds **1** and **2** and verapamil as revertant positive control for 15 min. Then, 2µM of rhodamine 123 was added and the cells were

further incubated at 37 °C in the dark for 1 h. After washing of the cells in PBS, the fluorescence was measured on cytometer. Analysis were performed selecting the excitation band centred at 488 nm and the emission at 530 nm, acquiring on logarithmic scale. Data were analysed by the WinMDI software and the fluorescence mean value of control samples was subtracted to the mean value of the treated ones.

*4.3.6 ATP assay*

The consumption of ATP was assessed by using ATPlite 1step luminescence kit (PerkinElmer Life Sciences), an ATP monitoring system based on firefly (Photinus pyralis) luciferase. The emitted light, produced by the reaction of ATP with added luciferase and D-luciferin, is proportional to the ATP concentration. In a 96-well black clear-bottom plate, according to the supplier's instructions, 100 µL of the reconstituted reagent were added to each well containing $2 \times 10^4$ cells, equilibrated at room temperature. Sensitive and MDR cells were exposed to 10µM of the compounds under test for 1h in a humidified atmosphere containing 5% $CO_2$ at 37 °C. Next, mammalian cell lysis solution (50µL) was added to all the wells, and the plates were agitated for 5 min on an orbital shaker. Substrate solution (50µL) was added to all wells, and the plates were stirred for another 5 min. Plates were dark adapted for 10 min, and luminescence was measured by System Sure II luminometer (Hygiena).

**Declaration of Competing Interest**

The authors declare no competing financial interests.

**References**

[1] F. Bray, J. Ferlay, I. Soerjomataram, R.L. Siegel, L.A. Torre, A. Jemal, Global cancer statistics 2018: GLOBOCAN estimates of incidence and mortality worldwide for 36 cancers in 185 countries, CA Cancer J. Clin. 68 (2018) 394.

[2] L. A. Mitscher, S. P. Pillai, E. J. Gentry, D. M. Shankel, Multiple drug resistance, Med. Res. Rev. 19 (1999) 467.

[3] N. A. Colabufo, F. Berardi, M. Contino, M. Niso, R. Perrone, ABC Pumps and their role in active drug transport. Curr. Top. Med. Chem. 9 (2009) 119.

[4] M. S. Jin, M. L. Oldham, Q. Zhang, J. Chen, Crystal structure of the multidrug transporter P-glycoprotein from *Caenorhabditis elegans*. Nature 490 (2012) 566.

[5] T. Suzuki, K. Nishio, S. Tanabe, The MRP family and anticancer drug metabolism. Curr. Drug Metab. 2 (2001) 367.

[6] S. Nobili, I. Landini, T. Mazzei, E. Mini, Overcoming tumor multidrug resistance using drugs able to evade P-glycoprotein or to exploit its expression. Med. Res. Rev. 32 (2012) 1220.

[7] A. H. Abuznait, A. Kaddoumi, Role of ABC Transporters in the Pathogenesis of Alzheimer's Disease. ACS Chem. Neurosci. 3 (2012) 820.

[8] P. Mistry, A. J. Stewart, W. Dangerfield, S. Okiji, C. Lidle, D. Bootle, J. A. Plumb, D. Templeton, P. Charlton, In vitro and in vivo reversal of P-glycoprotein-mediated multidrug resistance by a novel potent modulator, XR9576. Cancer Res. 61 (2001) 749.

[9] A. H. Dantzig, R. I. Shepard, J. Cao, K. I Law, W. J. Ehlhardt, T. M. Boughman, T. F. Bumol, J. J. Starling, Reversal of P-glycoprotein-mediated multidrug resistance by a potent cycloprpyldibenzosuberane modulator LY335979. Cancer Res. 56 (1996) 4171.

[10] A. Seelig, E. Landwojtowicz, Structure–activity relationship of P-glycoprotein substrates and modifiers. Eur. J. Pharm. Sci. 12 (2000) 31.

[11] K. M. Pluchino, M. D. Hall, A. S. Goldsborough, R. Callaghan, M. M. Gottesman, Collateral sensitivity as a strategy against cancer multidrug resistance. Drug Resist. Updat. 15 (2012) 98.

[12] A. Bisi, S. Gobbi, A. Rampa, F. Belluti, L. Piazzi, P. Valenti, N. Gyemant, J. Molnár, New potent P-glycoprotein inhibitors carrying a polycyclic scaffold. J. Med. Chem. 49 (2006) 3049.

[13] A. Bisi, S. Gobbi, L. Merolle, G. Farruggia, F. Belluti, A. Rampa, J. Molnar, E. Malucelli, C. Cappadone, Design, synthesis and biological profile of new inhibitors of multidrug resistance associated proteins carrying a polycyclic scaffold. Eur. J. Med. Chem. 92 (2015) 471.

[14] A. Bisi, R. L. Arribas, M. Micucci, R. Budriesi, A. Feoli, S. Castellano, F. Belluti, S. Gobbi, C. de Los Rios, A. Rampa, Polycyclic maleimide-based derivatives as first dual modulators of neuronal calcium channels and GSK-3β for Alzheimer's disease treatment. Eur. J. Med. Chem. 163 (2019) 394.

[15] A. Bisi, A. Mokhtar Mahmoud, M. Allará, M. Naldi, F. Belluti, S. Gobbi, A. Ligresti, A. Rampa, Polycyclic maleimide-based scaffold as new privileged structure for navigating the cannabinoid system opportunities. ACS Med. Chem. Lett. 10 (2019) 596.

[16] F. Bonvicini, I. Manet, F. Belluti, S. Gobbi, A. Rampa, G. A. Gentilomi, A. Bisi, Targeting the bacterial membrane with a new polycyclic privileged structure: a powerful tool to face staphylococcus aureus infections. ACS Infect. Dis. 5 (2019) 1524.

[17] R. Patel, S. W. Park, An evolving role of piperazine moieties in drug design and discovery. Mini-Rev. Med. Chem. 13 (2013) 1579.

[18] A. Bisi, M. Meli, S. Gobbi, A. Rampa, M. Tolomeo, L. Dusonchet, Multidrug resistance reverting activity and antitumor profile of new phenothiazine derivatives. Bioorg. Med. Chem. 16 (2008) 6474.

[19] E. Bonandi, M. S. Christodoulou, G. Fumagalli, D. Perdicchia, G. Rastelli, D. Passarella, The 1,2,3-triazole ring as a bioisostere in medicinal chemistry. Drug Disc. Today, 22 (2017) 1572.

[20] Y. Liu, M. Paige, T. T. Olson, N. Al-Muhtasib, T. Xie, S. Hou, M. P. White, A. Cordova, J. L. Guo, K. J. Kellar, Y. Xiao, M. L. Brown Synthesis and pharmacological characterization of new neuronal nicotinic acetylcholine receptor ligands derived from Sazetidine-A. Bioorg. Med. Chem. Lett. 24 (2014) 2954.

[21] F. Seghetti, R. M. C. Di Martino, E. Catanzaro, A. Bisi, S. Gobbi, A. Rampa, B. Canonico, M. Montanari, D. V. Krysko, S. Papa, C. Fimognari, F. Belluti. Curcumin-1,2,3-triazole conjugation for targeting the cancer apoptosis machinery. Molecules, 25 (2020) 3066.

[22] Z. Xu, S.-J. Zhao, Y. Liu. 1,2,3-Triazole-containing hybrids as potential anticancer agents: current developments, action mechanisms and structure-activity relationships. Eur. J. Med. Chem. 183 (2019) 111700.

[23] S. Bova, S. Saponara, A. Rampa, S. Gobbi, L. Cima, F. Fusi, G. Sgaragli, M. Cavalli, C. de los Rios, J. Striessnig, A. Bisi, Anthracene based compounds as new L-type $Ca^{2+}$ channel blockers: design, synthesis, and full biological profile. J. Med. Chem. 52 (2009) 1259.

[24] C. Menendez, A. Chollet, F. Rodriguez, C. Inard, M. R. Pasca, C. Lherbet, M. Baltas, Chemical synthesis and biological evaluation of triazole derivatives as inhibitors of InhA and antituberculosis agents. Eur. J. Med. Chem. 52 (2012) 275.

[25] V. Lopes-Rodrigues, A. Di Luca, J. Mleczko, P. Meleady, M. Henry, M. Pesic, D. Cabrera, S. van Liempd, R. T. Lima, R. O'Connor, J. M. Falcon-Perez, M. H. Vasconcelos, Identification of the metabolic alterations associated with the multidrug resistant phenotype in cancer and their intercellular transfer mediated by extracellular vesicles, Sci. Rep. 7 (2017) 44541.

[26] J. S. Lee, K. Paull, M. Alvarez, C. Hose, A. Monks, M. Grever, A. T. Fojo, S. E. Bates, Rhodamine efflux patterns predict P-glycoprotein substrates in the National Cancer Institute drug screen. Mol. Pharmacol. 46 (1994) 627.

[27] Molinspiration: Calculation of Molecular Properties and Bioactivity Score, Molinspiration Cheminformatics, http://www.molinspiration.com/cgi-bin/properties (accessed July 2019).

[28] E. Teodori, M. Contino, C. Riganti, G. Bartolucci, L. Braconi, D. Manetti, M. N. Romanelli, A. Trezza, A. Athanasios, O. Spiga, M. G. Perrone, R. Giampietro, E. Gazzano, M. Salerno, N. A. Colabufo, S. Dei, Design, synthesis and biological evaluation of stereo- and regioisomers of amino aryl esters as multidrug resistance (MDR) reversers. Eur. J. Med. Chem. 182 (2019) 111655.

[29] A. Alam, R. Küng, J. Kowal, R. A. McLeod, N. Tremp, E. V. Broude, I. B. Roninson, H. Stahlberg, K. P. Locher. Structure of a zosuquidar and UIC2-bound human-mouse chimeric ABCB1. Proc. Natl. Acad. Sci. U. S. A. 115 (2018) E1973-E1982;

[30] S. Dei, L. Braconi, A. Trezza, M. Menicatti, M. Contino, M. Coronnello, N. Chiaramonte, D. Manetti, M. G. Perrone, M. N. Romanelli, C. Udomtanakunchai, N. A. Colabufo, G. Bartolucci, O. Spiga, M. Salerno, E. Teodori Modulation of the spacer in N,N-bis(alkanol)amine aryl ester heterodimers led to the discovery of a series of highly potent P-glycoprotein-based multidrug resistance (MDR) modulators. Eur. J. Med. Chem. 172 (2019) 71.

[31] E. E. Chufan, K. Kapoor, H. M. Sim, S. Singh, T. T. Talele, S. R. Durell, S. A. Ambudkar. Multiple transport-active binding sites are available for a single substrate on human P-glycoprotein (ABCB1). PLoS One 8 (2013) e82463.

[32] J. Li, K. F. Jaimes, S. G. Aller. Refined structures of mouse P-glycoprotein. Protein Sci. 23 (2014), 34.

[33] L. Braconi, G. Bartolucci, M. Contino, N. Chiaramonte, R. Giampietro, D. Manetti, M. G. Perrone, M. N. Romanelli, N. A. Colabufo, C. Riganti, S. Dei, E. Teodori. 6,7-Dimethoxy-2-phenethyl-1,2,3,4-tetrahydroisoquinoline amides and corresponding ester isosteres as multidrug resistance reversers. J. Enzyme Inhib. Med. Chem. 35 (2020) 974.

[34] A. R. Safa, Identification and characterization of the binding sites of P-glycoprotein for multidrug resistance-related drugs and modulators. Curr. Med. Chem. Anticancer Agents, 4 (2004) 1.

[35] G. Janson, C. Zhang, M. G. Prado, A. Paiardini, PyMod 2.0: improvements in protein sequence-structure analysis and homology modeling within PyMOL. Bioinformatics 33 (2017) 444.

[36] R. A. Laskowski, M. W. MacArthur, D. S. Moss, J. M. Thornton, PROCHECK: a program to check the stereochemical quality of protein structures. J. Appl. Crystallogr. 26 (1993) 283.

[37] S. Jo, T. Kim, V. G. Iyer, W. Im, CHARMM-GUI: A web-based graphical user interface for CHARMM. J. Comput. Chem. 29 (2008) 1859.

[38] G. M. Morris, H. Ruth, W. Lindstrom, M. F. Sanner, R. K. Belew, D. S. Goodsell, A. J. Olson, Software news and updates AutoDock4 and AutoDockTools4: automated docking with selective receptor flexibility. J. Comput. Chem. 30 (2009) 2785.

[39] S. Kim, J. Chen, T. Cheng, A. Gindulyte, J. He, S. He, Q. Li, B. A Shoemaker, P. A Thiessen, B. Yu, L. Zaslavsky, J. Zhang, E. E Bolton, PubChem 2019 update: improved access to chemical data. Nucleic Acids Res. 47 (2019) D1102–D1109.

[40] N. M. O'Boyle, M. Banck, C. A. James, C. Morley, T. Vandermeersch, G. R. Hutchison, Open Babel: an open chemical toolbox. J. Cheminform. 3 (2011) 33.

[41] M. R. Koebel, G. Schmadeke, R. G. Posner, S. Sirimulla, AutoDock VinaXB: Implementation of XBSF, new empirical halogen bond scoring function, into AutoDock Vina. J. Cheminform. 8 (2016) 27.

[42] K. C. Hsu, Y. F. Chen, S. R. Lin, J. M. Yang, Igemdock: A graphical environment of enhancing gemdock using pharmacological interactions and post-screening analysis. BMC Bioinformatics 12 (2011) S33.

[43] S. Salentin, S. Schreiber, V. J. Haupt, M. F. Adasme, M. Schroeder, PLIP: Fully automated protein-ligand interaction profiler. Nucleic Acids Res. 43 (2015) W443.

[44] O. Wesołowska, J. Wiśniewski, K. Środa-Pomianek, A. Bielawska-Pohl, M. Paprocka, D. Duś, N. Duarte, M. U. Ferreira, K. Michalak, Multidrug resistance reversal and apoptosis induction in human colon cancer cells by some flavonoids present in citrus plants. Nat. Prod. 75 (2012) 1896.